Doctoral Forum on Vacuum Electronics (FVE 2017)

22–23 August 2017

Design and simulation of the high-frequency structure for a G-band extended interaction klystron

Linlin Hu[1,2], Zaojin Zeng[1], Hongbin Chen[1], Guowu Ma[1], Fanbao Meng[1]

[1]*Institute of Applied Electronics, China Academy of Engineering Physics, Mian Yang, Sichuan, People's Republic of China*
[2]*Graduate School, China Academy of Engineering Physics, Beijing, People's Republic of China*
E-mail: hulinlin2016@163.com

Published in *The Journal of Engineering*; Received on 8th February 2018; Accepted on 28th February 2018

Abstract: The G-band spectrum has been demonstrated to be the frequency of the next generation of space-borne and ground-based cloud radar for its higher spatial resolution. Extended interaction klystron (EIK) is one of the most suitable sources for the radar due to its longer lifetime and higher power compared with similar devices. The design and particle simulation of high-frequency structure for G-band EIK are presented in this study. The structure employs multiple resonant cavities, and each cavity adopts the ladder-type multi-gap structure. The cavities are operating at 2π mode considering the machinability. The simulation result indicates that the amplifier could generate a power of 125 W at 237.5 GHz when driven by a 20 kV, 200 mA round beam and 100 mW input power. This work will be of great potential to develop the G-band EIK with power above 100 W.

1 Introduction

The extended interaction klystron (EIK), combining the advantages of klystrons and travelling-wave tubes, is a novel compact amplifier with higher gain and broader bandwidth compared with conventional klystrons. It is well-suitable to operate at millimetre-wave, sub-millimetre-wave or THz band [1]. Today, EIKs have been demonstrated to be of great potential in many applications, such as meteorological survey, active denial, biomedicine, atmospheric sensing, communications, near-object analysis [2–4]. For instance, the W-band EIKs developed by Communications and Power Industries Inc. have been operating at Cloudsat satellite for cloud profile measurement for more than ten years. The peak power of Cloudsat EIK is 1.9 kW with duty cycle 3%. It has been demonstrated that G-band spectrum is the logical choice for the next generation of cloud profiling radar (CPR) for its higher spatial resolution [5]. G-band CPRs can significantly improve current profiling capabilities in boundary layer clouds, cirrus and mid-level ice clouds, and precipitating snow. However, the peak power of EIK for G-band CPR is required to reach 100 W level.

Here, the design and particle simulation of the high-frequency structure of a G-band EIK is presented. The EIK is expected to generate signals with a power over 125 W at 237.5 GHz by a 20 kV, 200 mA electron beam. The corresponding gain is 31 dB.

2 Cavity design

Target design parameters of G-band EIK are presented in Table 1. In order to realise the effective long-distance application for detection, imaging, and communication, the power of G-band EIK is required to exceed 100 W. As the frequency reaches the sub-millimetre-waveband, the electron efficiency of vacuum electronic devices is generally only about 2% level. So, we expect the efficiency could be >2.5% to constrain the source power below 4 kW. In consideration of practical application and system compatibility, the beam voltage could not exceed 20 kV, and the beam current is expected to utilise the quantity as small as possible. Meanwhile, as the power of the feed signal source devised by a solid-state circuit is limited at 100 mW level, the gain of EIK should be over 30 dB.

The multi-gap resonant cavities topology is utilised to achieve high power at G-band [2, 6, 7]. The proposed interaction structure is a ladder-type circuit as shown in Fig. 1. The structure of EIK is composed of three 9-gap resonant cavities. The input cavity, middle cavity and output cavity are based on the 9-gap ladder-type cavity as shown in Fig. 2. The input power transmitted by the standard WR4.0 waveguide is coupled into the input cavity through a tiny rectangular aperture. The linear pencil electron beam passes all the three cavities through a tiny round channel. The primary structure sizes, such as gap width d, gap period p, gap depth a, match cavity height h, beam radius r_c and so on are determined by many factors, such as resonant frequency, operating mode, beam parameters, interaction capability and vice versa. As the G-band high-power EIK has no bandwidth requirement, a relatively simple trade-off between power output, gain and fabrication practicalities should be considered to select the appropriate structure size.

Generally, the operating mode of the cavity is the π mode or 2π mode. Compared with the 2π mode, the π mode possesses higher coupling coefficient but less interaction impedance R/Q [6, 7]. Moreover, the period length of πmode is half of the 2π mode at the same operating voltage that means the π mode structure is more compact and more beneficial to beam transmission. However, the initial evaluation indicated that the period of π mode would be 0.17 mm at the designated voltage and frequency. This results in gap width <0.10 mm. For the state-of-art processing technique, the dimensions of the groove structure, beyond the capability of traditional fabrication techniques, could only be fabricated by an ultra-precise technique like LIGA and nano-CNC [8]. However, if we choose the 2π mode, the gap width could be optimised over 0.10 mm, the structure could be fabricated by precise CNC technique [9]. So, considering the machinability, cost and cycle, the operating mode of G-band EIK is adopted 2π mode.

The power of EIK is proportional to the factor M^2R/Q according to the klystron theory, and thus the structure size and gap number are optimised to achieve the maximum value of factor M^2R/Q. As

doi: 10.1049/joe.2018.0109

Table 1 Design parameters of G-band EIK

No.	Parameter	Target value
1	voltage	20 kV
2	current	200 mA
3	electron efficiency	>2.5%
4	input power	100 mW
5	output power	>100 W
6	gain	>30 dB

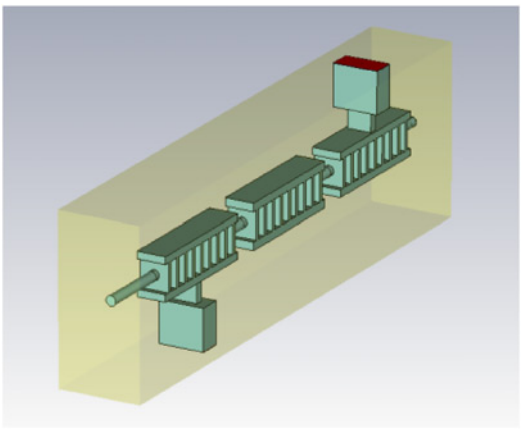

Fig. 1 *Simulation model of the designed G-band EIK in CST*

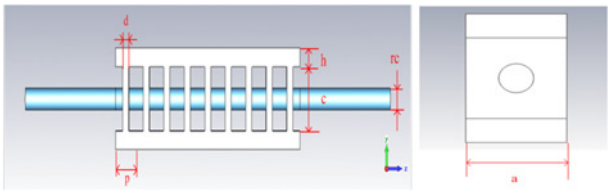

Fig. 2 *Schematic drawing of the ladder-type 9-gaps structure*

the field distribution is uniform in each gap for the 2π mode, we could simulate the parameters of the single-gap cavity to complete the optimisation. Fig. 3 shows the relation curves of interaction impedance R/Q versus gap width and factor M^2R/Q versus gap-width for the single-gap cavity, which indicates that although the R/Q is increasing with the gap-width, the factor M^2R/Q has an optimal value at a gap width of 0.12 mm.

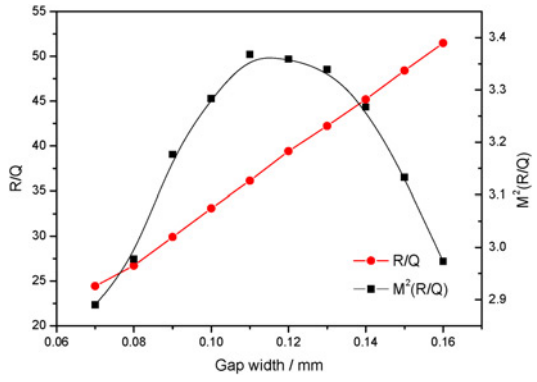

Fig. 3 *Relation curve of R/Q and M^2R/Q with gap width in the single-gap cavity*

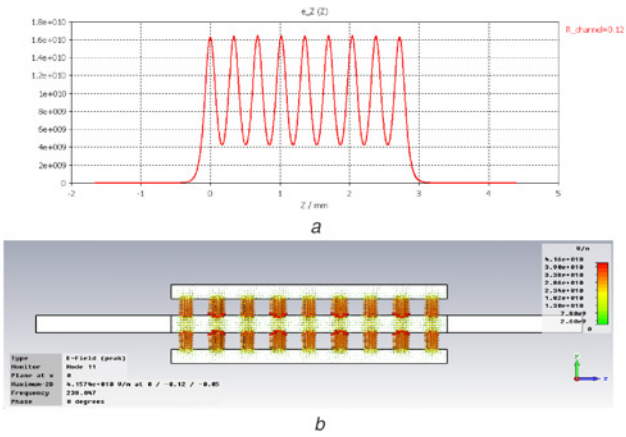

Fig. 4 *Field distribution plot of the middle 9-gap cavity of 2π eigenmode*
a Axial electronic field amplitude distribution in the cavity
b Electronic field vector plot in the cavity

Furthermore, the optimal gap number is determined 9 by calculating the M^2R/Q value of the multi-gap cavities with different gap numbers. The field amplitude distribution of 2π eigenmode in the 9-gap cavity is shown in Fig. 4, indicating that the field amplitude in the gaps is uniform in the ladder resonant structure. This merit ensures high interaction impedance R/Q in spite of low coupling coefficient and thereby ensures considerable M^2R/Q value. When the conductivity of oxygen-free high-conductivity copper is set 3.2×10^7 S/m based on the practical testing [10], the intrinsic factor Q_0 of the cavity is only 440. The coupling coefficient M and interaction impedance R/Q of the 9-gap cavity calculated by the following equations (1) and (2) are 0.32 and 295 Ω, respectively. The factor M^2R/Q is 30.

$$M = \frac{\left|\int_{-\infty}^{\infty} E_z e^{j\beta_n z}\,dz\right|}{\int_{-\infty}^{\infty} |E_z|\,dz} \tag{1}$$

$$R/Q = \frac{\left(\int_{-\infty}^{\infty} E_z\,dz\right)^2}{2\varpi_0 W} \tag{2}$$

3 3D particle-in-cell (PIC) simulation

The preliminary PIC simulation has been carried out by commercial PIC software, CST-PS and professional code, Magic. In the particle simulation, the device is driven by a 20 kV, 200 mA round beam transported using an 8 kG longitudinal magnetic field and the injected power is 100 mW. The hot-cavity frequency of the input cavity is 237.5 GHz when the reflection signal at the input port is minimum. The frequency of middle cavity and the distance between cavities have been optimised to maximum the harmonic current component, and the ultimate first harmonic current could

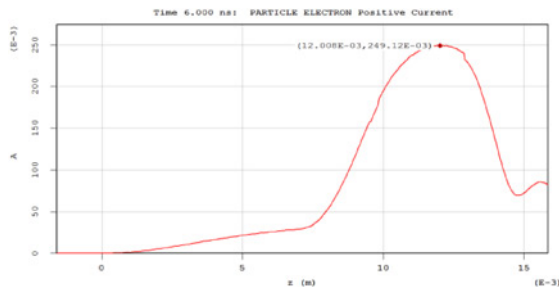

Fig. 5 *Harmonic current distribution along the axis*

doi: 10.1049/joe.2018.0109

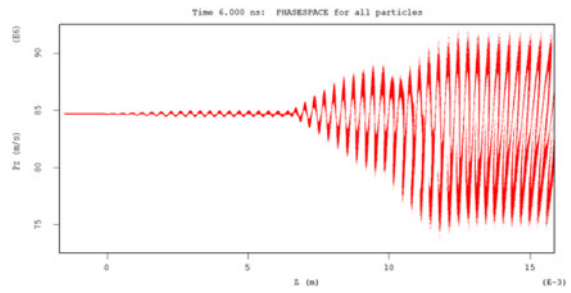

Fig. 6 *Snapshot of particle momentum in the axial direction*

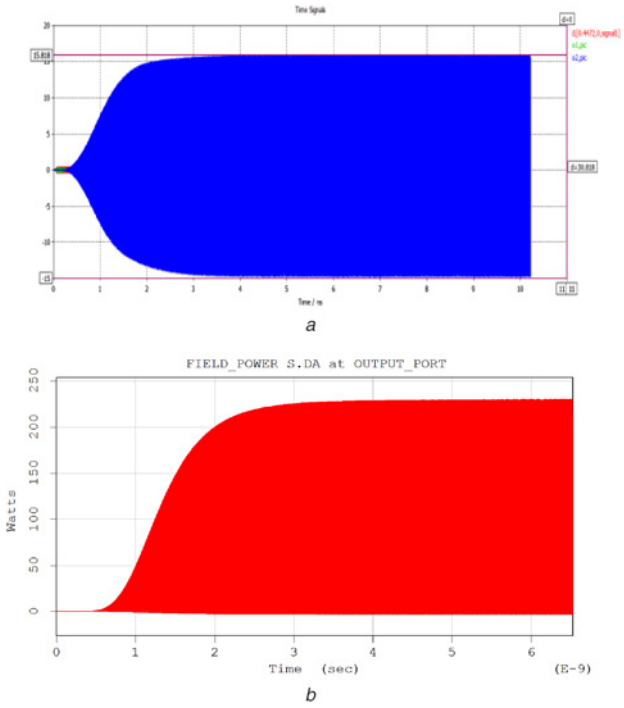

Fig. 7 *Signal waveform at input and output ports*
a Output signal waveform simulated by CST-PS
b Output transient power waveform simulated by Magic

reach about 250 mA, i.e. the modulation depth of 125%. The harmonic current distribution is shown in Fig. 5, and the synchronous particle momentum distribution is shown in Fig. 6.

The signals at the input port and output port simulated by CST-PS are shown in Fig. 7*a*, which indicate the equivalent voltage signal at the output port is 15.8 V, and so the output power achieved is ~125 W. The corresponding gain is 31 dB and electron efficiency ~3.1%. The PIC simulation results are consistent with Magic simulation as shown in Fig. 7*b*.

4 Conclusion

The design of a three-cavity high-frequency structure for high-power G-band EIK is presented. The cavities are operating in the 2π mode in consideration of the machinability. Compared with the π mode, the 2π mode has the advantage of larger gap-width with the capability of precise CNC fabrication, and the field amplitude in the gaps is uniform ensuring higher interaction impedance R/Q and considerable M^2R/Q to realise high gain amplification in spite of lower coupling. In the particle simulation, the structure generates 125 W power at 237.5 GHz when driven by a 20 kV, 200 mA round beam and 100 mW input power. Further optimisations are still undergoing, and these early works are promising for developing the 100 W G-band EIK.

5 References

[1] Steer B., Roitman A., Horoyski P., *ET AL.*: 'Advantages of extended interaction klystron technology at millimetre and sub-millimetre frequencies'. 2007 16th IEEE Int. Pulsed Power Conf., Albuquerque, NM, USA, 2007, pp. 1049–1053

[2] Roitman A., Berry D., Steer B.: 'State-of-the-art W-band extended interaction klystron for the CloudSat program', *IEEE Trans. Electron Devices*, 2005, **52**, (5), pp. 895–898

[3] Kemp T.F., Dannatt H.R.W., Barrow N.S., *ET AL.*: 'Dynamic nuclear polarization enhanced NMR at 187 GHz/284 MHz using an extended interaction klystron amplifier', *J. Magn. Reson.*, 2016, **265**, (1), pp. 77–82

[4] Steer B., Roitman A., Horoyski P., *ET AL.*: 'Millimeter-wave extended interaction klystrons for high power ground, airborne and space radars'. 41st European Microwave Conf., Manchester, UK, December 2011, pp. 984–987

[5] Battaglia A., Westbrook C.D., Kneifel S., *ET AL.*: 'G band atmospheric radars: new frontiers in cloud physics', *Atmos. Meas. Tech.*, 2014, **7**, (6), pp. 321–375

[6] Nguyen K.T., Pershing D., Wright E.L., *ET AL.*: 'Sheet-beam 90 and 220 GHz extend-interaction-klystron designs'. 8th IEEE Int. Vacuum Electronics Conf., Kitakyushu, Japan, July, 2007, pp. 193–194

[7] Pasour J., Wright E., Nguyen K.T., *ET AL.*: 'Demonstration of a multi-kilowatt, solenoidally focused sheet beam amplifier at 94 GHz', *IEEE Trans. Electron Devices*, 2014, **61**, (6), pp. 1630–1636

[8] Joye C.D., Cook A.M., Calame J.P., *ET AL.*: 'Demonstration of a high power, wideband 220-GHz traveling wave amplifier fabricated by UV-LIGA', *IEEE Trans. Electron Devices*, 2014, **61**, (6), pp. 1672–1678

[9] Xu A., Zhou Q. F., Yan L., *ET AL.*: 'Initial experimental study on 0.22THz folded waveguide TWT', *High Power Laser Part. Beams*, 2013, **25**, (11), pp. 2954–2958

[10] Xu A., Hu L. L., Yan L., *ET AL.*: 'Design and machining of components of 0.22THz folded waveguide travelling wave tube', *High Power Laser Part. Beams*, 2012, **4**, (9), pp. 2135–2140